Linear Integrated Optics in 3C Silicon Carbide

FRANCESCO MARTINI,[1] AND ALBERTO POLITI[1,*]

[1] *Department of Physics and Astronomy, University of Southampton, Southampton, SO17 1BJ, United Kingdom*
[*] *A.Politi@soton.ac.uk*

Abstract: The development of new photonic materials that combine diverse optical capabilities is needed to boost the integration of different quantum and classical components within the same chip. Amongst all candidates, the superior optical properties of cubic silicon carbide (3C SiC) could be merged with its crystalline point defects, enabling single photon generation, manipulation and light-matter interaction on a single device. The development of photonics devices in SiC has been limited by the presence of the silicon substrate, over which thin crystalline films are heteroepitaxially grown. By employing a novel approach in the material fabrication, we demonstrate grating couplers with coupling efficiency reaching -6 dB, sub-μm waveguides and high intrinsic quality factor (up to 24,000) ring resonators. These components are the basis for linear optical networks and essential for developing a wide range of photonics component for non-linear and quantum optics.

OCIS codes: (130.3120) Integrated optics devices; (130.3130) Integrated optics materials; (130.4310) Nonlinear.

References and links

1. J. L. O'Brien, A. Furusawa, and J. Vučković, "Photonic quantum technologies," Nature Photonics **3**, 687–695 (2009).
2. M. Davanco, J. Liu, L. Sapienza, C.-Z. Zhang, J. V. D. M. Cardoso, V. Verma, R. Mirin, S. W. Nam, L. Liu, and K. Srinivasan, "A heterogeneous iii-v/silicon integration platform for on-chip quantum photonic circuits with single quantum dot devices," arXiv preprint arXiv:1611.07654 (2016).
3. F. De Leonardis, R. A. Soref, and V. M. Passaro, "Dispersion of nonresonant third-order nonlinearities in silicon carbide," Scientific Reports **7** (2017).
4. I. Wu and G. Guo, "Second-harmonic generation and linear electro-optical coefficients of SiC polytypes and nanotubes," Physical Review B **78**, 035447 (2008).
5. L. G. Helt, M. Liscidini, and J. E. Sipe, "How does it scale? comparing quantum and classical nonlinear optical processes in integrated devices," J. Opt. Soc. Am. B **29**, 2199–2212 (2012).
6. C. A. Husko, A. S. Clark, M. J. Collins, A. De Rossi, S. Combrié, G. Lehoucq, I. H. Rey, T. F. Krauss, C. Xiong, and B. J. Eggleton, "Multi-photon absorption limits to heralded single photon sources." Scientific reports **3**, 3087 (2013).
7. X. Tang, K. G. Irvine, D. Zhang, and M. G. Spencer, "Linear electro-optic effect in cubic silicon carbide," Applied Physics Letters **59**, 1938 (1991).
8. A. Vonsovici, G. T. Reed, and A. G. Evans, "β-SiC-on insulator waveguide structures for modulators and sensor systems," Materials Science in Semiconductor Processing **3**, 367–374 (2000).
9. A. L. Falk, B. B. Buckley, G. Calusine, W. F. Koehl, V. V. Dobrovitski, A. Politi, C. a. Zorman, P. X.-L. Feng, and D. D. Awschalom, "Polytype control of spin qubits in silicon carbide." Nature communications **4**, 1819 (2013).
10. F. Fuchs, V. a. Soltamov, S. Väth, P. G. Baranov, E. N. Mokhov, G. V. Astakhov, and V. Dyakonov, "Silicon carbide light-emitting diode as a prospective room temperature source for single photons." Scientific reports **3**, 1637 (2013).
11. S. Castelletto, B. C. Johnson, V. Ivády, N. Stavrias, T. Umeda, a. Gali, and T. Ohshima, "A silicon carbide room-temperature single-photon source." Nature materials **13**, 151–6 (2014).
12. G. Calusine, A. Politi, and D. D. Awschalom, "Cavity-Enhanced Measurements of Defect Spins in Silicon Carbide," Physical Review Applied **6**, 014019 (2016).
13. V. Bratus', R. Melnik, S. Okulov, V. Rodionov, B. Shanina, and M. Smoliy, "A new spin one defect in cubic SiC," Physica B: Condensed Matter **404**, 4739–4741 (2009).
14. N. Son, E. Sorman, W. Chen, M. Singh, C. Hallin, O. Kordina, B. Monemar, E. Janzen, and J. Lindstrom, "Dominant recombination center in electron-irradiated 3c sic," Journal of applied physics **79**, 3784–3786 (1996).
15. C.-M. Zetterling, ed., *Process Technology for Silicon Carbide Devices* (Institution of Engineering and Technology, 2002).
16. S. Nishino, H. Suhara, H. Ono, and H. Matsunami, "Epitaxial growth and electric characteristics of cubic sic on silicon," Journal of applied physics **61**, 4889–4893 (1987).
17. J. Cardenas, M. Yu, Y. Okawachi, C. B. Poitras, R. K. Lau, A. Dutt, A. L. Gaeta, and M. Lipson, "Optical nonlinearities in high-confinement silicon carbide waveguides," Optics letters **40**, 4138–4141 (2015).

18. M. Bosi, G. Attolini, M. Negri, C. Frigeri, E. Buffagni, C. Ferrari, T. Rimoldi, L. Cristofolini, L. Aversa, R. Tatti, and R. Verucchi, "Optimization of a buffer layer for cubic silicon carbide growth on silicon substrates," Journal of Crystal Growth **383**, 84–94 (2013).
19. R. Anzalone, G. D'arrigo, M. Camarda, C. Locke, S. Saddow, and F. La Via, "Advanced residual stress analysis and fem simulation on heteroepitaxial 3c–sic for mems application," Journal of Microelectromechanical Systems **20**, 745–752 (2011).
20. Q. Li, M. Davanço, and K. Srinivasan, "Efficient and low-noise single-photon-level frequency conversion interfaces using silicon nanophotonics," Nature Photonics **10**, 406–414 (2016).
21. X. Tang, K. Wongchotigul, and M. G. Spencer, "Optical waveguide formed by cubic silicon carbide on sapphire substrates," Applied Physics Letters **58**, 917 (1991).
22. F. Xia, M. Rooks, L. Sekaric, and Y. Vlasov, "Ultra-compact high order ring resonator filters using submicron silicon photonic wires for on-chip optical interconnects," Optics express **15**, 11934–11941 (2007).
23. Q. Xu, B. Schmidt, S. Pradhan, and M. Lipson, "Micrometre-scale silicon electro-optic modulator." Nature **435**, 325–7 (2005).
24. Z. Yang, P. Chak, A. D. Bristow, H. M. van Driel, R. Iyer, J. S. Aitchison, A. L. Smirl, and J. E. Sipe, "Enhanced second-harmonic generation in AlGaAs microring resonators." Optics letters **32**, 826–8 (2007).
25. P. S. Kuo, J. Bravo-Abad, and G. S. Solomon, "Second-harmonic generation using-quasi-phasematching in a gaas whispering-gallery-mode microcavity," Nature communications **5** (2014).
26. X. Lu, J. Y. Lee, P. X.-L. Feng, and Q. Lin, "Silicon carbide microdisk resonator." Optics letters **38**, 1304–6 (2013).
27. J. Cardenas, M. Zhang, C. T. Phare, S. Y. Shah, C. B. Poitras, B. Guha, and M. Lipson, "High q sic microresonators," Optics express **21**, 16882–16887 (2013).
28. T. Shoji, T. Tsuchizawa, T. Watanabe, K. Yamada, and H. Morita, "Low loss mode size converter from 0.3 μm square si wire waveguides to singlemode fibres," Electronics Letters **38**, 1669–1670 (2002).
29. A. Bozzola, L. Carroll, D. Gerace, I. Cristiani, and L. C. Andreani, "Optimising apodized grating couplers in a pure soi platform to −0.5 db coupling efficiency," Opt. Express **23**, 16289–16304 (2015).
30. W. S. Zaoui, A. Kunze, W. Vogel, M. Berroth, J. Butschke, F. Letzkus, and J. Burghartz, "Bridging the gap between optical fibers and silicon photonic integrated circuits." Optics express **22**, 1277–86 (2014).
31. K. M. Jackson, J. Dunning, C. A. Zorman, M. Mehregany, and W. N. Sharpe, "Mechanical properties of epitaxial 3c silicon carbide thin films," Journal of microelectromechanical systems **14**, 664–672 (2005).
32. P. Rabiei, W. Steier, C. Zhang, and L. Dalton, "Polymer micro-ring filters and modulators," Journal of Lightwave Technology **20**, 1968–1975 (2002).
33. G. Calusine, A. Politi, and D. D. Awschalom, "Silicon carbide photonic crystal cavities with integrated color centers," Applied Physics Letters **105**, 011123 (2014).
34. S. Yamada, B.-S. Song, S. Jeon, J. Upham, Y. Tanaka, T. Asano, and S. Noda, "Second-harmonic generation in a silicon-carbide-based photonic crystal nanocavity." Optics letters **39**, 1768–71 (2014).
35. D. O. Bracher and E. L. Hu, "Fabrication of High- Q Nanobeam Photonic Crystals in Epitaxially Grown 4H-SiC," Nano Letters **15**, 6202–6207 (2015).
36. F. Van Laere, T. Claes, J. Schrauwen, S. Scheerlinck, W. Bogaerts, D. Taillaert, L. O'Faolain, D. Van Thourhout, and R. Baets, "Compact focusing grating couplers for silicon-on-insulator integrated circuits," IEEE Photonics Technology Letters **19**, 1919–1921 (2007).

1. Introduction

The development of new photonic platforms for quantum technologies poses strict requirements in the choice of optical materials, given the range of functionalities needed [1]. For example, the necessity of interfacing atom-like emitters as stationary qubits and the use of non-centrosymmetric crystal structures for non-linear processes are required in the same physical system. Quantum emitters coupled with an integrated cavity would overcome the challenge of embedding single photon sources and provide non-linear interactions between single photons, both cornerstones to achieve a multitude of quantum applications. Non-centrosymmetry is a prerequisite for fast integrated reconfigurable optical circuit and, together with a wide electronic bandgap, for efficient frequency conversion and generation of non-classical states of light. Currently, many materials are optimized to demonstrate individual components for quantum optics, but the road to achieve hybrid integrated devices [2] is not clear. Monolithic integration would solve the scalability problem of devices exploiting quantum optics phenomena.

The unique properties of 3C Silicon Carbide have recently attracted strong interest for matching all the essential requirements. Its non-centrosymmetric crystal structures grants both third-order [3] and second-order non-linear effects, with a significant $\chi^{(2)}$ susceptibility of 34 pm/V [4].

The high refractive index of 2.6, indispensable for deep integration of photonic components and small modal volume in resonators, together with the wide electronic bandgap of 2.3 eV, could allow efficient non-linear optics processes, like frequency conversion and non-classical generation of light, without incurring in multiple photon absorption that limits silicon quantum photonics [5, 6]. Furthermore, the high electro-optic coefficient could be used for the fabrication of fast lossless Pockels modulators [7, 8].

The presence of point defects in the SiC crystalline structure [9] provides additional capabilities for quantum technology - including single photon generation [10, 11] and the engineering of light interaction with electronic spins [12]. Among other defects, SiC colour centers based on Ky5 defects display features similar to diamonds NV centers [13] with the convenience of a zero-phonon-line emission in the near-infrared (1100 nm) [14], closer to the telecom wavelengths, and the possibility of being integrated with semiconductor devices thanks to an advanced fabrication technology [15]. Although most SiC polytypes show similar properties, including the presence of quantum emitters, 3C SiC has the advantage of being available as thin layers epitaxially grown on a silicon substrate [16]. This is a key advantage for optical applications as it avoids additional fabrication steps needed to create thin layers from thick crystals [17]. The heteroepitaxial growth of 3C SiC comes at expences of a lower crystal quality due to the lattice mismatch between 3C SiC and Si, expecially at the interface between the two materials [18, 19]. Coupling of color centers with non-linear optical components can provide wavelength converters [20] to the telecommunication band for efficient communication, or to other frequencies, for interfacing with diverse quantum systems. However, to take advantage of all these properties, a fully scalable photonics platform in 3C SiC, able to integrate different components, is needed.

The development of photonics structures in 3C SiC is limited by the presence of a Si substrate, since its higher refractive index makes the confinement of light impossible. Solutions to this problem have been demonstrated creating a bottom cladding formed by oxygen implantation [8] or using a sapphire substrate in order to achieve SiC on insulator structures [21]. However, these demonstrations provided waveguide confinement with high modal-area geometry. The development of sub-μmeter cross-section waveguides would provide tighter confinement, essential for enhancing light-matter interactions and deep integration of optical devices. Strong confinement is also required to provide compact optical resonators, an essential component for multiple linear applications, from filtering to switches [22, 23]. Furthermore, in materials with $\bar{4}$ crystal symmetry as 3C SiC, circular cavities have been demonstrated to provide efficient second order non-linearities: light propagating through a resonator experiences crystallographic inversions that can be used to achieve quasi-phase matching [24, 25]. Suspended cavities were demonstrated with high quality factor [26, 27], but were not integrated with bus waveguides, essential for scalable optical circuits. Moreover, these high-multimode cavities are hard to optimally couple to the fundamental mode and limit the possibility of fully engineering the mode dispersion. Here we demonstrate all fundamental components for linear photonics, including sub-μmeter cross-section waveguide in 3C SiC at telecom wavelength, grating couplers and first-mode resonance in micro ring resonators using a novel and scalable technology. The process makes use of two steps of electron beam lithography that removes the underlying Si substrate and suspends in air all the optical components. Both single-mode (SM) and multi-mode (MM) platforms are developed, showing coupling efficiency (CE) for gratings couplers (including losses in tapering) as high as -6 dB for both SM and MM structures and intrinsic quality factors up to 24,000. Improvements in the processing, tailored to minimize scattering losses, could increase the applications of SiC photonics.

2. Simulations

The high refractive index of SiC is fully exploited by our technology using air as cladding and sub-μm cross-section of the waveguides. A mode analysis of the structures is performed for

the fundamental TE mode, reported in Fig. 1, showing effective index n_{eff} of 1.88 (SM) and 2.25 (MM) for 480x400 nm and 670x700 nm sizes, respectively. The possibility of engineering the waveguide dimensions for the MM waveguides can improve the propagation losses by diminishing the roughness scattering thanks to a major confinement of the mode inside the material and the consequent reduction of the field at the SiC-air boundary. The n_{eff} difference between the fundamental and higher order modes is kept wide enough for avoiding cross-mode field leakage, especially in small-radii bending of waveguides. The high n_{eff} values of both structures are evidence of a thigh light confinement, essential for integrating photonics components in a small area and achieving the minimum modal volume in resonators.

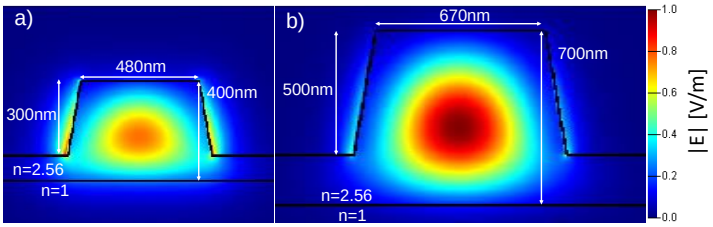

Fig. 1. Normalized electric field intensity for the first TE mode in SM (a) and MM (b) waveguides.

The high field confinements in waveguides is a problem for coupling light from an optical fiber due to a small field overlap between the two modes that would cause high insertion losses. In order to overcome this problem, mode converters can minimize the modal mismatch in edge-coupling systems [28] showing high CE but requiring further processes (as dicing and polishing, that compromise the throughput of the process), in general combined with lensed fibers. Alternatively, grating couplers are one of the most used component in silicon photonics since they can be integrated in different parts of the chip (thanks to the vertical coupling) with a higher spatial tolerance in the alignment. Gratings remove the need of polishing steps often used to maximize performances in edge-coupling systems and can be easily scaled to couple tens of waveguides using standard v-grove fiber arrays.

The versatility of our technology offers the possibility to use both techniques, slightly changing the process list in order to insert the polishing step in case of edge coupling. We focus here on grating couplers, since they best take advantage of the presence of a second step of electron-beam lithography to achieve the highest CE. By implementing the model [Fig. 2(a)] in a 2D-FTDT simulator, we optimized the grating period, etch depth and filling factor for maximizing the CE from a 8°-tilted single mode fiber injecting TE-polarized light. Fig. 2(b) reports the simulated CE versus wavelength for the best period (794 nm and 720 nm for SM and MM waveguide, respectively), etch depth (162 nm and 320 nm for SM and MM waveguide, respectively) and filling factor (0.457 and 0.417 for SM and MM waveguide, respectively). For both structures we considered a sidewall angle of 80°, consistent with our process technology, and a refractive index of 2.6. Despite the lack of a back reflector, often used in SOI technology, the SM grating coupler reaches a high CE of -4.4 dB at 1550 nm and a wide 3 dB bandwidth of 88 nm. On the other side, the uniform grating coupler for the MM platform shows reduced CE of -7.7 dB with the fundamental mode, and a similar bandwidth of 74 nm.

In order to match the spatial distribution of the scattered light from the grating with the gaussian shape of the fiber mode and improve the CE, it is possible to optimize the position and size of each post (apodized grating coupler). The parameter space, already composed by the etch depth (ED) and the position of the fiber with respect to the grating coupler (F_{pos}), is increased by two times the number of posts composing the grating coupler: each post i adds a period p_i and a size s_i [Fig. 2(a)]. In a similar way to references [29, 30], we developed a four-steps

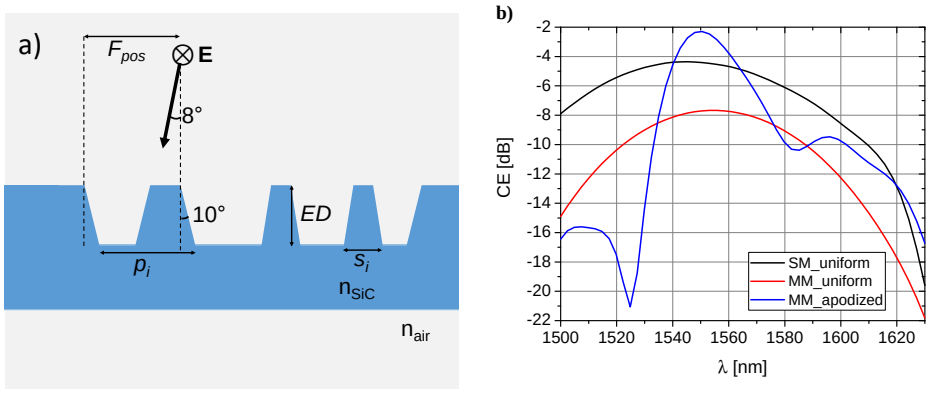

Fig. 2. (a) Schematic of an apodized grating coupler. (b) Coupling efficiency versus wavelength from 2D-FDTD simulation of grating couplers optimized for SM and MM waveguides.

algorithm to optimize the CE: 1) In a first step, we optimize the uniform grating coupler for a given etch depth in order to find the best period p and size s. 2) From the previous step, the algorithm simulates structures sweeping sequentially the value of all s_i for a set of periods close to p for each post i. The parameters are saved only if they perform with an higher CE at 1550 nm than the previous saved solution. The procedure is repeated until the solution converges. 3) In this step, every saved position p_i and sizes s_i are mutated by different random values between ±2 nm and the new grating coupler is simulated. Once again, the parameters are saved only if they perform with an higher CE and the procedure is repeated until the solution converges. 4) By changing ED of the grating of 10 nm steps and repeating step 3), it is possible to determine the etch depth that delivers the highest CE. At each step, F_{pos} is swept in order to maximize CE. The optimization can be constrained by process limitations in step 3): for minimum post size of 100 nm and distance between two post of 50 nm, the retrieved post positions and sizes are reported in Table 1 for an etch depth of 320nm. This level of constrains does not affect drastically the CE since the reduction from the optimal design lies in a few percent, and makes the designed structure feasible with the fabrication process described below. The simulated CE for MM waveguides is reported in Fig. 2 and it improves for the apodized case reaching a value of -2.3 dB at expense of the bandwidth, that reduces to 27 nm. Rather than simply maximizing the CE at 1550 nm, the described algorithm can be used to optimize different figure of merits of the grating depending on the requirements of the photonic device.

3. Experimental results

In order to fabricate photonics components in SiC, we developed the fabrication procedure depicted in Figs. 3(a)-3(f). The SiC layer, heteroepitaxially grown on a Si <001> substrate, is purchased from *NOVASIC* with a chemical-mechanically polished surface. As the first step, the SiC film is thinned down to the desired waveguide thickness (400 nm and 700 nm for SM and MM waveguide, respectively) by dry etching, while a first electron beam lithography step is performed to define the waveguide width of 480 nm (SM) and 670 nm (MM) using CSAR62 resist [Fig. 3(b)]. The pattern is subsequently transferred to a 100 nm aluminum hardmask by dry etching in order to guarantee sufficient selectivity during the high-power ICP-RIE SiC etch based on fluorine chemistry (SF_6), Fig. 3(c). The SiC layer is etched 300 nm and 500 nm for SM and MM waveguides, respectively, and a thin SiC membrane is left in order to provide mechanical support once the Si substrate is removed. In a second fabrication flow, both grating coupler

Table 1. Positions and sizes resulting from the apodization algorithm for the MM structure, with a refractive index of 2.6 and an etch depth of 320 nm

$1 < i < 10$		$11 < i < 20$	
p_i [nm]	s_i [nm]	p_i [nm]	s_i [nm]
562.2	482.0	824.7	381.8
652.5	233.1	961.7	232.9
791.8	449.8	542.2	492.2
711.0	235.1	688.9	232.9
617.6	472.8	734.0	614.0
793.3	379.4	571.2	308.7
777.3	232.9	947.0	288.4
667.7	609.6	640.6	589.7
812.1	232.9	758.9	616.8
500.1	428.8	516.5	254.2

grooves and holes in the membrane are patterned by etching the SiC layer for 162 nm (SM) and 320 nm (MM), Figs. 3(d) and 3(e). The etch depths are chosen to produce the optimum CE for the gratings couplers, while being greater than the membrane thickness, ensuring that the holes expose part of the silicon substrate. In this way, a XeF_2 vapor etch can be performed to undercut the Si substrate, suspending the photonics components and generating the maximum refractive index contrast achievable [Fig. 3(f)]. Fig. 3(g) shows a 45°-tilted SEM picture of a suspended MM ring resonator resulting from the described fabrication flow. The optical-microscope image of the final device is reported in Fig. 4(a) and depicts a suspended area of ~40 μm around the waveguides. The extremely high Young's modulus of SiC [31] ensures large suspensions without incurring in the membrane cracks or deformations.

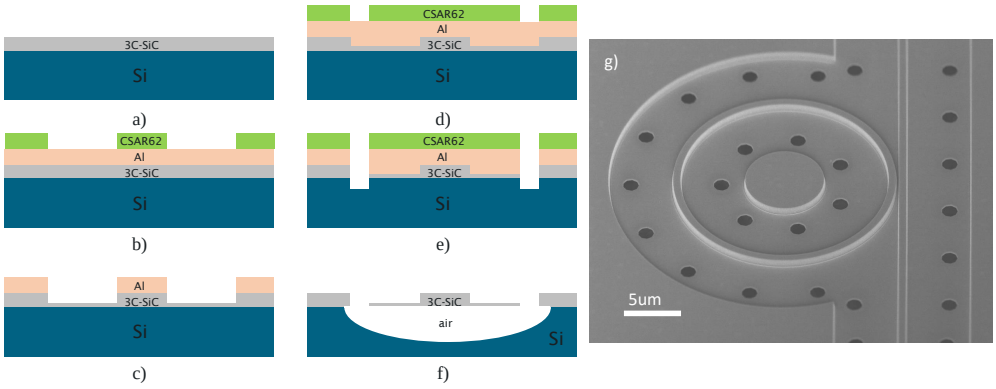

Fig. 3. Schematic representation of the fabrication process (a)-(f). 45° SEM view of a MM ring resonator (g).

The photonics components are characterized in TE polarization using a CW laser (*Santec TSL-510*) tunable across the telecom band (1500-1630 nm) and a polarization-maintaining fiber array. Following the layout of the fabricated optical circuit [Fig. 4(a)], light is injected using the uniform grating coupler for the SM waveguide and the apodized grating coupler for the MM waveguide. Both gratings are optimized for the refractive index measured by ellypsometry on the two different wafers used for the fabrication of SM and MM waveguides. Since the lateral dimension of the grating is 20 μm to maximize the overlap with single mode fibers,

mode converters are employed to adiabatically reshape the mode at the grating to the SM and fundamental MM ones. Numerical simulations show conversion loss lower than 0.15 dB for the fabricated length of 800 μm and 490 μm (SM and MM case, respectively).

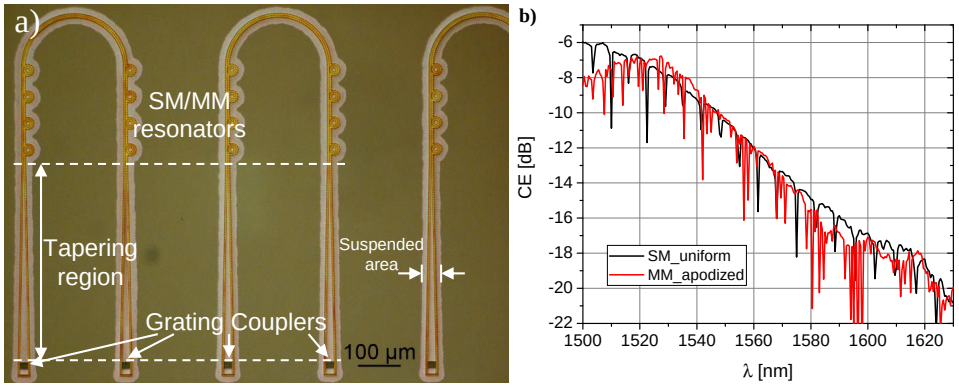

Fig. 4. Optical microscope image of the sample layout (a). Experimental characterization of fabricated SM and MM grating coupler together with mode converter (b).

We characterize the performance of the grating couplers by measuring the transmission of SM and MM devices. Since the linear losses calculated below are valid only for the SM (MM) part of the circuit in Fig. 4(a), the grating plus tapering section are characterized as a single coupling component. In Fig. 4(b), the total CE for the grating-taper component is reported for both the SM and MM case. The CE is ~-6 dB (-6.8 dB) at 1500 nm (1527.5 nm) and the half width at half maximum is ~38 nm (~18 nm) for the SM (MM) platform. The shift in wavelength of the measured CE compared to the simulation results, is ascribed to fabrication imperfections given by the high etching rate (giving an error on waveguide thickness and ED parameter) and a small difference between the actual refractive index of the sample and the one used for simulations. Both effects are amplified by the high refractive index contrast.

Ring resonators provide a direct way to retrieve linear losses of waveguides from the measured quality factor [32]. Thanks to the high confinement, we fabricated ring resonators with small radius of 10 μm (MM) and 20 μm (SM and MM) that are simulated to exhibit small excess bending losses. In the same sample, different gaps between bus waveguides and rings are fabricated in order to tune the coupling strength with the resonators and determine the coupling condition. Fig. 5 shows measurements of transmission versus wavelength for a SM-20μm ring [Fig. 5(a)], MM-10μm ring [Fig. 5(b)] and MM-20μm ring [Fig. 5(c)]. For the SM resonance, the intrinsic quality factor is calculated as 9,100 corresponding to linear losses of 58 dB/cm. When the field is more confined inside the material (MM waveguides) the scattering losses reduces and the intrinsic quality factor improves up to 20,000 (25 dB/cm) for the 10 μm ring. This is further shown from Fig. 5(c), where the bigger radius decreases the field overlap with the sidewall roughness and the intrinsic quality factor reaches 24,000 (21 dB/cm). Further increasing the radius of the resonator does not provide any significant improvement in the propagation losses. Since the mode intensity at the sidewall is still non-zero for the MM waveguide [Fig. 1(b)], it is possible that the reported value of the losses is still not limited by material absorption. The improvements in the losses for the MM structures are also partially explained by the reduction of the field intensity in bottom part of the SiC layer, where the high density of defects generated during the crystal growth increases the material absorption.

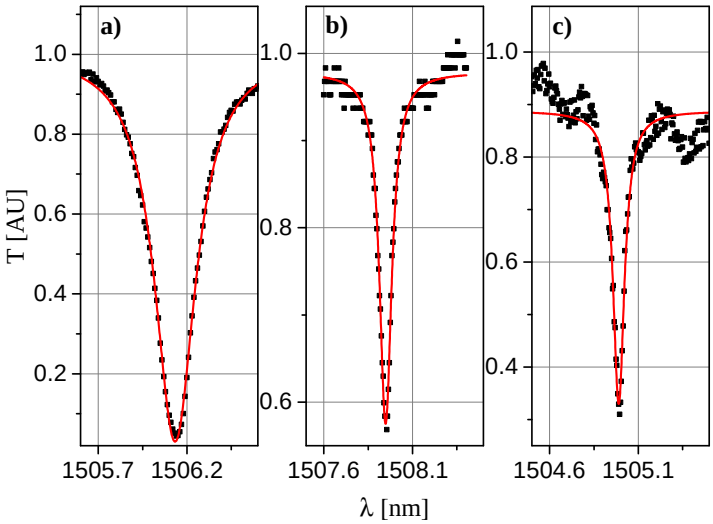

Fig. 5. Measured high-Q resonance of different ring resonators (black dots) and lorentzian best-fit (red line): 20 μm ring realized with SM waveguide (a), 10 and 20 μm ring realized with MM waveguides (b and c, respectively). All the rings are in the undercoupled condition.

4. Conclusions

3C SiC is particularly suitable for non-linear and quantum photonics due to its rare characteristics. The presence of a Si substrate, needed for heteroepitaxially growing the crystalline SiC layer, hampered the development of basic photonics components needed for a multitude of optical processes. Thanks to a new fabrication approach, that removes the underlying substrate by employing two steps of electron beam lithography, both SM and MM photonic platforms were realized in a fully scalable manner. This technology can easily be integrated with photonic crystal cavities, a key component for exploiting SiC point defects [33] and low power non-linear interaction [34], and be extended to other heteroepitaxially grown materials, such as hexagonal SiC films created by electrochemical etching [35] or GaAs membranes. The fabricated couplers show CE around -6 dB when considering grating efficiency and taper propagation loss (in the order of 1-2 dB considering MM propagation losses). This value can be improved using self-focusing gratings [36] that do not require long mode converters, increasing transmission and reducing the footprint of the optical devices. The characterized ring resonators demonstrated high intrinsic quality factors up to 24,000. Even though the reported values of quality factor are sufficient to demonstrate non-linear effects like efficient frequency conversion, improving the propagation losses would open the possibility to use SiC for scalable quantum optical interconnections. Additional steps in the fabrication procedure, including roughness reduction by oxidization or the deposition of a cladding to decrease the high index contrast, could target the scattering loss by reducing the roughness effects and improve the quality factor of the resonators. The reported results demonstrate a fundamental step in the development of SiC photonics and open the way for the integration of a variety of classical and quantum devices.

Funding

Engineering and Physical Sciences Research Council (EPSRC) EP/P003710/1.

Acknowledgments

We acknowledge support from the Southampton Nanofabrication Centre for the development of SiC technology. We thank Roman Buck for experimental support. All data supporting this study are openly available from the University of Southampton repository at http://dx.doi.org/10.5258/SOTON/D0039